Separation and Purification Technology 376 (2025) 133985

Contents lists available at ScienceDirect

Separation and Purification Technology

journal homepage: www.elsevier.com/locate/seppur

Eco-techno-economic analysis of onboard membrane carbon capture and storage systems considering CO_2/N_2 and CO_2/O_2 selectivity improvements

Hongkyoung Shin [a], Abduljelil Worku Sabir [b], Juyoung Oh [c], Pyung Soo Lee [b,*], Youngsub Lim [a,d,e,**]

[a] Department of Naval Architecture and Ocean Engineering, Seoul National University, 1 Gwanak-ro, Gwanak-gu, Seoul 08826, Republic of Korea
[b] School of Chemical Engineering and Material Science, Chung-Ang University, Seoul 05974, Republic of Korea
[c] Korea Institute of Energy Research, 152 Gajeong-ro Yuseong-gu, Daejeon 34129, Republic of Korea
[d] Research Institute of Marine Systems Engineering, Seoul National University, 1 Gwanak-ro, Gwanak-gu, Seoul 08826, Republic of Korea
[e] Institute of Engineering Research, Seoul National University, 1 Gwanak-ro, Gwanak-gu, Seoul 08826, Republic of Korea

ARTICLE INFO

Editor: Gaohong He

Keywords:
Onboard CCS
Membrane-based CO_2 capture
CO_2 Liquefaction
Selectivity
Process design
GHG intensity

ABSTRACT

The shipping industry aims to achieve net zero emissions, and compact-sized membrane-based onboard carbon capture and storage systems can be a feasible solution. However, most previous studies have overlooked the importance of CO_2/O_2 separation performance, leading to higher energy consumption and operating expenditures. In this study, a three-stage membrane carbon capture system was integrated with a precooled Linde–Hampson liquefaction process to minimize CO_2 avoidance costs while adhering to the FuelEU Maritime regulations. Two case studies assessed the impact of CO_2/N_2 and CO_2/O_2 selectivity improvements: one with a fixed greenhouse gas intensity target (62.90 g_{CO2eq}/MJ, 2040–44 target) and another with varying targets. The results show that enhancing selectivity for not only CO_2/N_2 but also CO_2/O_2 is essential for developing cost-effective and energy-efficient onboard membrane carbon capture and storage systems, making it a feasible solution.

1. Introduction

The maritime sector is facing the new challenge of decarbonization, which has resulted in the implementation of various regulations, such as the Energy Efficiency Design Index (EEDI), Energy Efficiency Existing Ship Index (EEXI), and Carbon Intensity Indicator (CII) [1]. The International Maritime Organization (IMO) has introduced the 2023 IMO GHG strategy to establish an intermediate trajectory toward achieving net zero emissions by 2050 [2,3] and is currently discussing specific measures [4,5]. In 2025, the FuelEU Maritime regulation is being implemented through a staged reduction approach as shown in Table 1. It assesses well-to-wake (WtW) greenhouse gas (GHG) emissions to reduce GHG emissions intensity by 80 % (18.23 g_{CO2eq}/MJ) by 2050, compared with the reference intensity of fossil fuels (91.16 g_{CO2eq}/MJ). Furthermore, ships that fail to comply with the GHG intensity limits will face mandatory penalties [6,7]. Stakeholders in the shipping industry must consider how to adhere to decarbonization regulations, as the transition to net zero is inevitable.

Integrating an onboard carbon capture and storage (OCCS) system on liquefied natural gas (LNG)-fueled ships can be a feasible option for meeting future environmental requirements [8–10]. LNG emits approximately 20 % less CO_2 than conventional heavy-fuel oil [11]; however, further efforts are required to reduce emissions. While alternative fuels can reduce GHG emissions, meeting immediate regulatory requirements is technically challenging due to the limited production of green fuels. Additionally, scaling up to achieve financial viability for marine transportation presents significant technological and economic challenges [12]. Moreover, alternative fuels involve uncertainties in supply and pricing, the need for infrastructure development, and fuel containment issues [13]. Therefore, OCCS can be a bridge technology to reduce CO_2 emissions from ships.

Prior studies on CO_2 capture have focused on amine-based chemical absorption, but it requires considerable vertical space, which could be troublesome on a ship with limited space [14]. Luo and Wang [15] investigated an onboard carbon capture and liquefaction system with 35

* Corresponding author.
** Corresponding author at: Department of Naval Architecture and Ocean Engineering, Seoul National University, 1 Gwanak-ro, Gwanak-gu, Seoul 08826, Republic of Korea.
E-mail addresses: leeps@cau.ac.kr (P.S. Lee), s98thesb@snu.ac.kr (Y. Lim).

https://doi.org/10.1016/j.seppur.2025.133985
Received 30 March 2025; Received in revised form 31 May 2025; Accepted 12 June 2025
Available online 13 June 2025

Nomenclature

Letters

A_{mem}	total membrane area (m^2)
$\dot{m}_{inlet}$	inlet molar flow (mol/s)
V_{std}	standard gas volume flow (m^3/s)
A	area (m^2)
Pr	pressure (bar)
V	volume (m^3)
M_{water}	removed water mass flow (kg/h)
P	permeability (Barrer)
PW	power (kW)

Abbreviations

ACAPEX	Annualized capital expenditure
AMP	2-amino-2-methyl-1-propanol
CAPEX	Capital expenditure
CII	Carbon Intensity Indicator
EEDI	Energy Efficiency Design Index
EEXI	Energy Efficiency Existing Ship Index
GHG	Greenhouse gas
GPU	Gas permeation unit
GTD	General Technical Data
GWP	Global warming potential
IMO	International Maritime Organization
JT	Joule–Thomson
LCO_2	Liquefied CO_2
LCV	Lower calorific value
LNG	Liquefied natural gas
MCR	Maximum continuous rating
MEA	Monoethanolamine
MEPC	Marine Environment Protection Committee
MGO	Marine gas oil
MTR	Membrane Technology and Research
O&M	Operation and maintenance
OCCS	Onboard carbon capture and storage
OPEX	Operating expenditure
OPS	Onshore power supply
PZ	Piperazine
SFOC	Specific fuel oil consumption
SGC	Specific gas consumption
TEA	Techno-economic analysis
TtW	Tank-to-wake
WtT	Well-to-tank
WtW	Well-to-wake

Table 1
GHG intensity reduction phases.

Year	Reduction rate (%)	GHG intensity limit (g_{CO2eq}/MJ)
2020	Reference value	91.16
2025	2	89.34
2030	6	85.69
2035	14.5	77.94
2040	31	62.90
2045	62	34.64
2050	80	18.23

wt% monoethanolamine (MEA) in 17 MW diesel-powered cargo ships. They reported that the absorber packing height and diameter were 12.5 and 4.9 m, respectively, and the stripper packing height and diameter were 6.5 and 2.1 m, respectively, to achieve a 90 % capture rate. Cho et al. [16] evaluated the carbon capture performance of a 20,020 kW crude oil tanker fueled by LNG, comparing 30 wt% MEA with a blended solvent of 27 wt% 2-amino-2-methyl-1-propanol (AMP) and 13 wt% piperazine (PZ). They found that the AMP-PZ blend offered economic advantages, with the absorber size measuring 15.0 m × 4.13 m and the stripper measuring 14.5 m × 1.35 m. A design with reduced height may be feasible. However, decreasing the height of the absorber packing can increase the energy demand for regeneration. Furthermore, insufficient packing height may hinder the achievement of the target capture rate [17].

Membranes with relatively compact sizes can be used for carbon capture, and much research has been conducted on these membranes. Literature acknowledges that the high separation performance of CO_2 and N_2 is essential for membrane CO_2 capture technologies to compete with traditional amine absorption methods [18–20]. Merkel et al. [20] and Lee et al. [21] considered the separation performance of CO_2 and N_2 in a binary mixture. Furthermore, Xu et al. [22] conducted a parametric study to examine CO_2/N_2 membrane separation performance in a post-combustion coal-fired plant, where the feed gases were CO_2 13.5 mol%, N_2 68.8 mol%, O_2 2.4 mol% H_2O 15.3 mol%. However, most studies have focused on enhancing CO_2/N_2 separation performance without considering oxygen.

Enhancing CO_2 and O_2 separation performance is crucial for onboard membrane carbon capture; however, its significance has not been overlooked. Notably, ship exhaust gas contains a significantly lower CO_2 mole fraction (2.5–6 mol%) and a higher O_2 mole fraction (9–15 mol%) than flue gas from onshore power plants [9,22,23]. Oh et al. [24] examined a ternary mixture of CO_2, N_2, and O_2 to simulate an LNG-fueled ship exhaust gas. While their study acknowledged the presence of O_2 in the gas composition, they did not address the challenges associated with CO_2/O_2 separation. Although CO_2 has a small kinetic diameter and high solubility in most membrane materials, its properties are only slightly superior to those of O_2, unlike N_2 [25,26]. As a result, CO_2/N_2 gas separation benefits from high selectivity, whereas improving CO_2/O_2 selectivity remains a significant challenge. Fig. 1 plots the selectivity of CO_2/N_2, O_2/N_2, and CO_2/O_2 from the accumulated experimental membrane database for polymer membranes up to 2018 [27]. These data indicate that technological advancements have improved CO_2/N_2 and O_2/N_2 selectivities, but CO_2/O_2 selectivity remained relatively unchanged. Therefore, in OCCS, where O_2 concentrations are high, low CO_2/O_2 selectivity is a critical factor in the development of an energy-efficient CO_2 capture system.

This study aims to identify the membrane separation performance that meets the FuelEU Maritime GHG intensity limits with a CO_2 avoidance cost comparable to that of alternative decarbonization technologies, typically ranging from $100–$300 per tonne of CO_2 avoided. A quaternary gas mixture of CO_2, N_2, O_2, and H_2O is used as the exhaust gas from a ship to reflect the operating conditions. Three-stage membrane-onboard carbon capture and liquefaction storage systems are designed and optimized to minimize CO_2 avoidance cost with given GHG reduction targets. Case studies are conducted to demonstrate the effect of improving the selectivity of CO_2/N_2 and CO_2/O_2, either separately or simultaneously.

2. Background

2.1. Membrane gas separation

Membrane-based gas separation for carbon capture offers operational simplicity, but faces challenges in achieving high selectivity and permeability. The separation process relies on sorption, diffusion, and desorption mechanisms. The key performance indicators of membrane

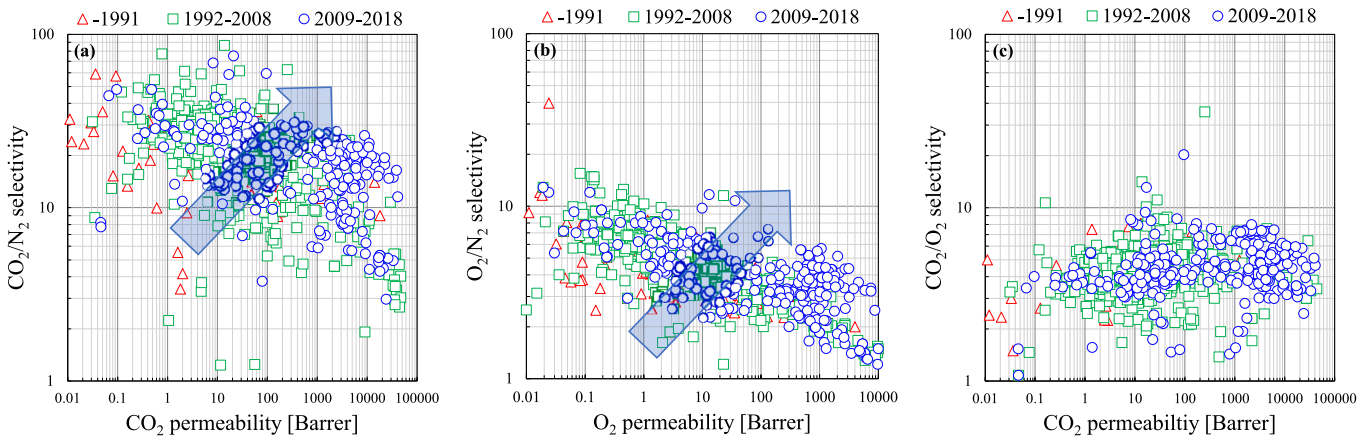

Fig. 1. Membrane separation performance curve: (a) CO_2/N_2; (b) O_2/N_2; (c) CO_2/O_2.

material, permeability, permeance, and selectivity, play a crucial role in determining gas separation efficiency. Permeance is defined as permeability divided by membrane thickness, where permeability represents the capacity of the membrane to allow gas flow, and selectivity quantifies its ability to distinguish between different gases, typically expressed as the ratio of their permeabilities. Designing polymer membranes for selective gas separation requires careful balancing of diffusivity and solubility to optimize the performance of the target gas. However, the intrinsic trade-off between permeability and selectivity poses a significant challenge, necessitating precise material design and optimization strategies.

Robeson et al. [25] developed permeability correlations based on extensive data on the permeabilities of gas-separated polymer membranes. Unlike the upper-bound results [28], which focus on maximum separation performance, this correlation serves as a benchmark for the performance of typical polymeric materials. It was established using data collected for various gas pairs, including He, H_2, O_2, N_2, CO_2, and CH_4. By plotting permeability on a log–log scale, the permeability correlation is expressed as Eq. (1).

$$P_j = kP_i^n \tag{1}$$

where P_j and P_i represent the permeabilities of gases i and j, respectively, with P_i indicates the more permeable gas.

In addition to membrane material properties, membrane system engineering plays a crucial role in optimizing gas separation performance. Even with lower-performance membrane materials, a well-engineered membrane system can enhance overall efficiency through strategic process design [29,30]. Key factors such as stage design, pressure ratios, flow patterns, and operational strategies can significantly impact separation effectiveness. Multi-stage or hybrid membrane systems, integration with compressors or vacuum pumps, and optimized module designs can help improve separation selectivity and reduce energy consumption. Therefore, a comprehensive approach that considers both membrane material development and system engineering is essential to achieve high-performance and energy-efficient membrane-based carbon capture.

2.2. CO_2 liquefaction process

CO_2 can be liquefied across various pressures, from the triple point at low pressure and low temperature (5.18 bar, −56.6 ℃) to the critical point at high pressure and high temperature (73.8 bar, 31.1 ℃). Low pressure reduces the energy needed for compression but requires a large liquefaction system. Its relatively high density makes it advantageous for transportation purposes. Conversely, high pressure demands a large compression system but allows for a small liquefaction system, resulting in a cost-effective option [31].

Various liquefaction cycles have been analyzed for the liquefaction of CO_2, as shown in Fig. 2 [32]. The Linde–Hampson cycle (Fig. 2a) is a simple process that uses low- and high-pressure compressors and a Joule–Thomson (JT) valve to achieve liquefaction. The Linde dual-pressure cycle (Fig. 2b) is a modified version of the Linde–Hampson system that uses two-stage vapor–liquid separation to reduce the required work. Compared to these systems, the precooled Linde–Hampson cycle (Fig. 2c) uses external refrigerants such as propane and ammonia to precool the compressed gas before it enters the heat exchanger. In the process, gas is first compressed and mixed with the precooled recycled gas from the separator. The mixed gas stream is further cooled through heat exchange with the external refrigerants. After passing through a Joule–Thomson JT valve, the precooled gas undergoes expansion, resulting in partial liquefaction. This system can improve liquid yield and reduce the life cycle cost (LCC).

2.3. Greenhouse gas assessment

According to the FuelEU Maritime Regulation, WtW GHG intensity represents life cycle GHG emissions, combining Well-to-Tank (WtT) and Tank-to-Wake (TtW) GHG emissions as shown in Eqs. (2)–(4) [6].

$$\mathrm{GHG_{WtW}}\left[\mathrm{g_{CO2eq}/MJ}\right] = f_{\mathrm{wind}} \bullet (\mathrm{GHG_{WtT}} + \mathrm{GHG_{TtW}}) \tag{2}$$

$$\mathrm{GHG_{WtT}} = \frac{\sum_i^n M_i \bullet \mathrm{CO_{2eqWtT,}}_i \bullet \mathrm{LCV}_i + \sum_k^c E_k \bullet \mathrm{CO_{2eqE,}}_k}{\sum_i^n M_i \bullet \mathrm{LCV}_i \bullet \mathrm{RWD}_i + \sum_k^c E_k} \tag{3}$$

where f_{wind} represents the wind-assisted propulsion reward factor, i is the fuel type used onboard, and n is the number of fuel types. M refers to the mass of the fuel,k represents the index for the onshore power supply (OPS) connection points, c denotes the total number of OPS connection points, LCV_i is the lower calorific value of fuel i, and $\mathrm{CO_{2eqWtT,}}_i$ represents the WtT GHG emission factor of fuel i. RWD is a reward factor applied to non-biological origin renewable fuels, E_k is the electricity delivered to the ship at k, and $\mathrm{CO_{2eqE,}}_k$ is the WtT GHG emission factor associated with E_k.

$$\mathrm{GHG_{TtW}} = \frac{\sum_i^n \sum_j^m M_{i,j}\left[\left(1-\frac{C_{\mathrm{slip},j}}{100}\right)\left(\sum_l C_{f,l,j} \bullet \mathrm{GWP}_l\right) + \frac{C_{\mathrm{slip},j}}{100}\left(\sum_l C_{sf,l,j} \bullet \mathrm{GWP}_l\right)\right]}{\sum_i^n M_i \bullet \mathrm{LCV}_i \bullet \mathrm{RWD}_i + \sum_k^c E_k} \tag{4}$$

where j represents the fuel consumer units such as the generator and main engine, and l denotes the GHGs (CO_2, CH_4, and N_2O). C_{slip} is a non-combusted fuel coefficient that accounts for fugitive and slipped emissions. GWP_l is the global warming potential over a 100-year horizon. C_f and C_{sf} denotes the TtW GHG emission factors of the combusted and

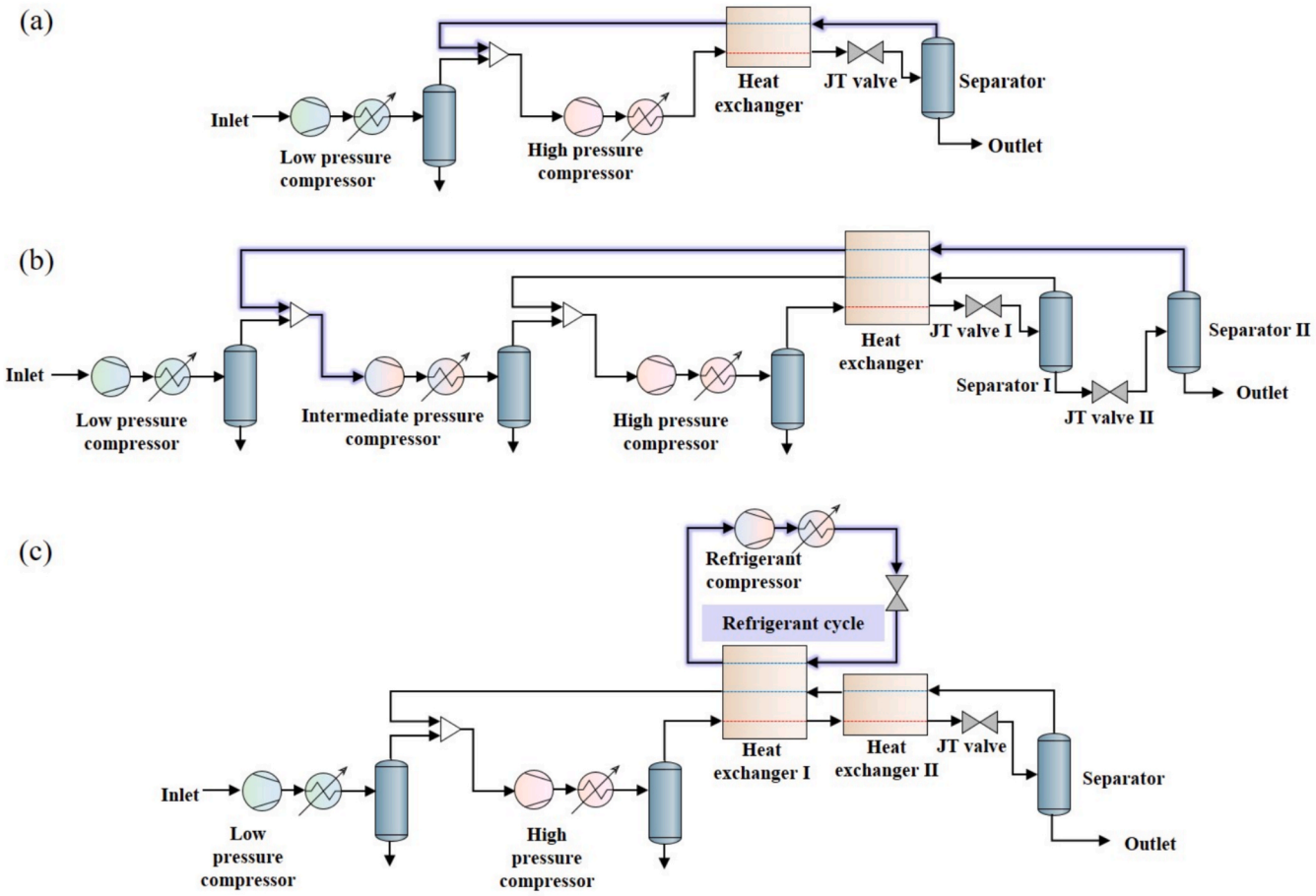

Fig. 2. CO_2 liquefaction systems: (a) Linde-Hampson; (b) Linde dual-pressure Hampson; (c) Precooled Linde-Hampson.

slipped fuels, respectively.

However, the current FuelEU Maritime framework does not consider the reduction in emissions achieved through carbon capture by ships. Oh et al. [33] presented modified the equation that accounts for both the amount of CO_2 captured and the additional CO_2 generated from the OCCS system as shown in Eq. (5).

$$GHG_{TtW} = \frac{\sum_i^n \sum_j^m \left(M_{i,j} \bullet \left(\sum_l C_{f,l,j} \bullet GWP_l\right) + M_{CO_2 gen,j}\right) + M_{CH_4} \bullet GWP_{CH_4} - M_{CO_2 cap}}{\sum_i^n (M_i \bullet LCV_i)} \quad (5)$$

The modified TtW GHG emissions were calculated by adding the $M_{CO_2 gen,j}$ from the operation of the main engine and OCCS system and subtracting the $M_{CO_2 gen,j}$. Instead of the slip term, C_{slip}, in the original FuelEU regulations, the actual amount of slipped methane obtained from the engine performance data was applied. M_{CH_4} represents the methane slip emissions from the combustion of LNG in the main engine.

3. Modeling and simulation

3.1. System definition

Fig. 3. shows the process flow diagram of the proposed OCCS system. In this study, a 6X72DF-2.1 iCER engine was selected and the exhaust gas data were estimated using WinGD General Technical Data (GTD) as shown in Table 2 [34]. The main engine load was estimated to be 50%, reflecting the average load derived from the engine load profile [14]. The exhaust gas from the engine was cooled to 40 ℃ in a direct contact cooler (DCC), modeled in Aspen Plus version 14 (Fig. 3a). The parameters of the DCC and conditions of the exhaust gas entering the membrane are listed in Table 3. After the DCC, the cooled exhaust gas was fed directly into the membrane separation process. After CO_2 separation in the first and second membrane stages (MEM1 and MEM2), the captured CO_2 stream containing impurities was directed to the liquefaction process (Fig. 3b). The CO_2 stream was liquefied through heat exchange with a low-temperature propane refrigerant and two-stage JT expansion. In the first expansion, the vapor phase separated in the first separator, which includes impurities such as N_2 and O_2, was recycled to the membrane separation process to enhance the purity of the liquefied CO_2 (LCO_2) stream.

3.2. Onboard membrane carbon capture process

The membrane carbon capture process was configured with a three-stage membrane layout (Fig. 3a) [21,35], and the process was modeled using Symmetry (Schlumberger/VMG) version 2023.3 software. A vacuum pump and cooler were installed downstream of each membrane stage to generate the required high-pressure gradient efficiently. The

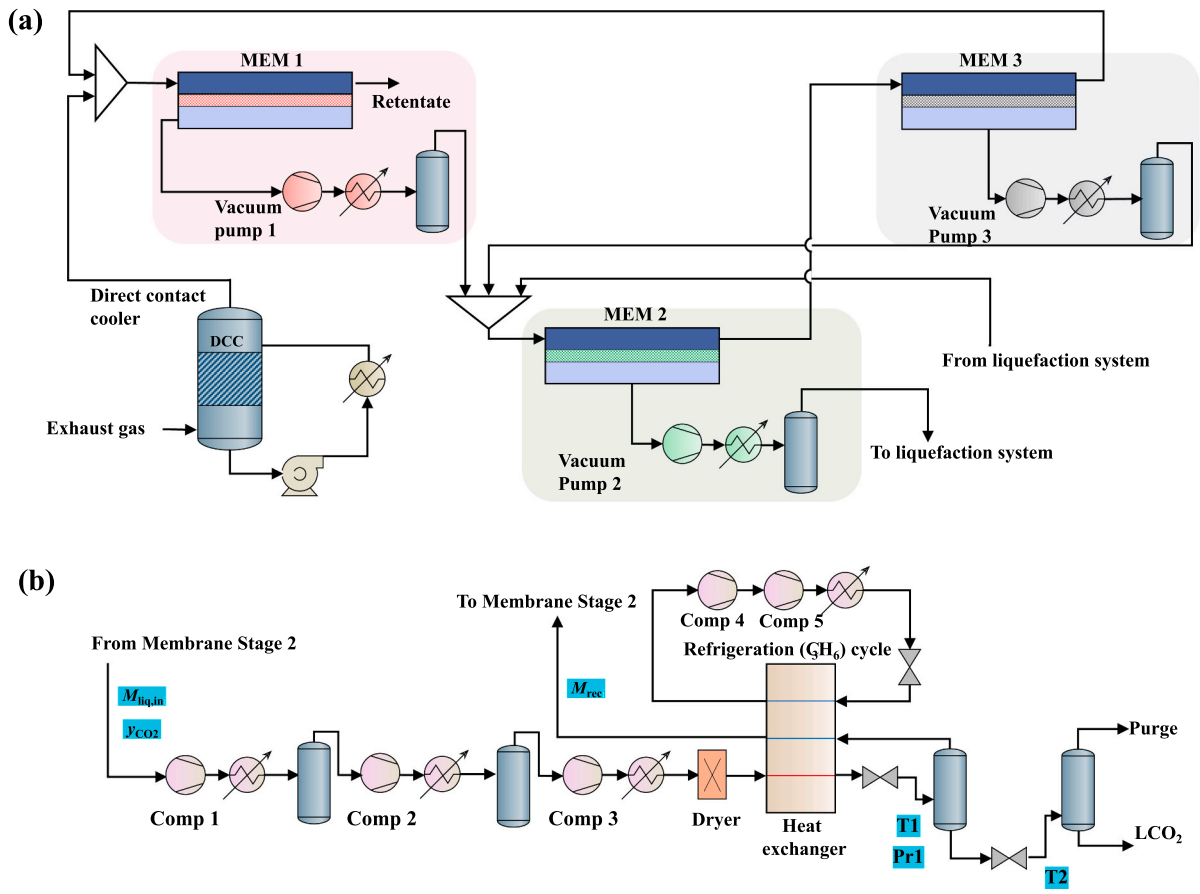

Fig. 3. Process flow diagram of the onboard membrane carbon capture and storage system: (a) Membrane capture; (b) Liquefaction.

Table 2
Information on the target engine.

Category	Unit	Value
Main engine fuel	–	LNG
Main engine	–	6X72DF-2.1
MCR	kW	18,200
Main engine load	%	50
SGC	g/kWh	134.9
SFOC	g/kWh	1.0
Methane slip	g_{CH4}/kWh	1.3

Table 3
Key parameters of the direct contact cooler (DCC) and exhaust gas conditions.

Category	Unit	Value
DCC diameter	m	2.58
DCC height	m	5
Exhaust gas flow after DCC	t/h	38.45
CO_2	mol%	5.35
H_2O	mol%	6.77
N_2	mol%	77.95
O_2	mol%	9.93
Exhaust gas temperature after DCC	℃	40
Exhaust gas pressure after DCC	bar	1.1

permeate was cooled to 35 ℃, and condensed water was removed [36,37]. As shown in Table 5, the flow configuration in the first-stage membrane was designed as a one-dimensional (1D) counter-current system to handle the large volumetric flow of CO_2 at low concentrations by maximizing the partial pressure difference—the primary driving force for CO_2 diffusion across the membrane. In contrast, 1D cross-flow configurations were employed in the second and third membrane stages, where the volumetric flow rate is significantly reduced due to upstream CO_2 removal. This approach allows for a more compact and modular system layout, while also simplifying operation and reducing the risk of membrane fouling [38]. In the current model, average stage-wise compositions were used instead of fully resolved axial concentration profiles. As a result, phenomena such as local concentration polarization, axial gradients, and boundary layer resistance were not explicitly captured. However, the system operates at moderate CO_2 purity levels (70–85 %) and spans a broad range of membrane performance parameters. These conditions are typically less sensitive to non-ideal effects [39]. Moreover, the use of a multistage membrane configuration with interstage mixing helps refresh the gas composition between stages, thereby mitigating purity losses associated with pressure drop and concentration polarization.

To determine membrane performance, the Robeson permeability correlation Eq. (1) was employed [25]. Although the Robeson upper bound [28] is widely referenced, it may be commercially impractical for process design. Therefore, the Robeson permeability correlation was selected because it more accurately reflects the performance of typical gas separation membranes and allows for a commercially viable process design. First, the CO_2 permeance was assumed, and the permeabilities and selectivities for N_2, O_2, and H_2O were subsequently calculated. The CO_2 permeability was determined considering a selective layer thickness

Table 4
nAnd ***k*** values for Eq. (1).

Gas pair	*n*	*k*
CO_2/N_2	1.1212	0.03419
CO_2/O_2	1.017	0.223

of 10^{-4} cm. The permeabilities and permeances of N_2 and O_2 were derived using the Robeson permeability correlation, as described in Eq. (1) and Table 4. A scaling factor was applied to the correlation to account for the improvement in selectivity, resulting in selectivity improvement rates of 10, 20, 30, and 100 %. Meanwhile, H_2O permeability was calculated using a fixed selectivity 0.7 [38]. The derived values were used to calculate the selectivities for each gas pair, assuming identical membrane performance across the 1st, 2nd, and 3rd stages. A pressure ratio of 11 was selected for all membrane stages, corresponding to a feed pressure of 1.1 bar and a permeate side of 0.1 bar. These operating conditions align with previous studies on membrane-based CO_2 capture systems [35,40]. This pressure ratio also falls within the optimal range of 10 to 15, as identified in the literature, which is effective for minimizing vacuum pump energy consumption while achieving a high CO_2 purity of up to 97 % [41]. The assumptions for membrane performance are summarized in Table 5.

3.3. CO_2 liquefaction process

Captured CO_2 must be liquefied for onboard storage. A precooled Linde–Hampson system with a propane refrigerant was utilized in this study (Fig. 3b) [32,42]. Following multistage compression (Comp 1–3), a molecular sieve dryer was used to remove moisture to prevent hydrate formation [43]. The high-pressure CO_2 stream exchanged heat with a low-temperature refrigerant and was expanded through a JT valve to be liquefied. A two-stage expansion and separation are used to get the liquefied CO_2 stream (LCO_2) at 15 bar. The key assumptions used in the liquefaction process are listed in Table 6.

3.4. Greenhouse gas emissions assessment

The GHG emissions evaluation was conducted based on the FuelEU Maritime regulations, with modifications to account for the CO_2 captured by the OCCS system and the additional emissions associated with its power requirements as shown in Eqs. (2)–(3) and (5) [6,33]. The global warming potential (GWP) 100 values for CH_4 and N_2O were set to 25 and 298, respectively [44]. The wind reward factor f_{wind} was set to 1 as wind-assisted propulsion was not considered. The values for calculating the GHG emissions are summarized in Table 7.

In the onboard process, CO_2 emissions include not only emissions from the main engine but also additional CO_2 emissions resulting from the power required to operate the OCCS system. The OCCS system requires significant power to run devices such as the membrane vacuum pump and compressor used in the liquefaction process. To meet these power requirements, a 4,350 kW MGO-fueled 5X35-B engine (WinGD) was selected as a generator, and the exhaust gas conditions were determined using WinGD GTD software. Based on the data, the CO_2 mass flow (M_{CO_2}) in the exhaust gas and fuel consumption (M_{fuel}) per generator power (PW_{gen}) were modeled using linear regression, as shown in Fig. 4.

The modeled M_{CO_2} was used to estimate the TtW emissions, whereas M_{fuel} was used to calculate both the WtT and TtW emissions. Considering all these factors, the total GHG emissions from the system, including those from OCCS operation, were comprehensively evaluated.

Table 5
Assumptions and specifications for the membrane capture process.

Category	Value	Remark
Mem1 flow pattern	Counter current	[38]
Mem2 flow pattern	Cross flow	[38]
Mem3 flow pattern	Cross flow	[38]
Outlet temperature of the cooler	35 ℃	[38]
Pressure ratio	11	[35,40,41]
Pump efficiency	85 %	–
CO_2 permeance	GPU	1000–3000
O_2 permeance	GPU	From Eq. (1) and Table 4 [25]
N_2 permeance	GPU	From Eq. (1) and Table 4 [25]
H_2O permeance	GPU	Calculated from selectivity
CO_2/H_2O selectivity	–	0.7 [38]
Membrane thickness	cm	10^{-4}

Table 6
Assumptions for CO_2 liquefaction process.

Category	Unit	Value
Refrigerant	–	Propane (C_3H_6)
LCO_2 storage pressure	bar	15
Minimum temperature approach of heat exchanger	℃	5
Outlet temperature of the cooler	℃	35
Pressure drop	bar	0
Compressor efficiency	%	85

Table 7
Values used to calculate GHG intensity [6,34].

Category	Unit	LNG	MGO
LCV	MJ/g_{Fuel}	0.05	0.0427
CO_{2eqWtT}	g_{CO2eq}/MJ	18.5	14.4
C_{fCO2}	g_{CO2}/g_{Fuel}	0.0	0.0
C_{fCH4}	g_{CH4}/g_{Fuel}	0.0	0.00005
C_{fN2O}	g_{N2O}/g_{Fuel}	0.00011	0.00018

3.5. Cost estimation

The cost of each piece of equipment in the process was calculated using the cost estimation formulas listed in Table 8. The total process lifetime was assumed to be 25 years, with membrane replacement scheduled every 5 years. The price of MGO fuel was set at $774/t, based on the 6-month average at the Port of Rotterdam as of July 2024. The CO_2 avoidance cost was determined considering the calculated equipment and fuel costs, which included the additional fuel consumption by the generator.

3.6. Optimization

To minimize CO_2 avoidance costs while complying with the FuelEU Maritime GHG intensity limits, optimization was performed using a mixed-integer genetic algorithm embedded in symmetry. The CO_2 permeance and stage cut of each membrane were considered as variables. In the liquefaction process, the pressure ratios of multiple CO_2 compressors and the pressure after the first JT valve were included as variables. The temperature of each stream after passing through the first and second JT valves was constrained to prevent the formation of dry ice. The target WtW GHG value was set at 62.90 g_{CO2eq}/MJ, which complies with the FuelEU Maritime regulations until 2044 and represents a 31 % reduction compared with the 2020 reference year [6]. Table 9 and Table 10 summarize the variables and constraints applied in the optimization.

4. Results and discussion

4.1. Specific energy consumption and CO_2 avoidance cost with fixed target greenhouse gas intensity

Fig. 5 illustrates the specific energy consumption (SEC) and CO_2 avoidance costs required to meet the GHG intensity limit of 62.90 g_{CO2eq}/MJ (the 2040–2044 target) as a function of improvements in CO_2/N_2 and CO_2/O_2 selectivity, based on Eq. (1) and Table 4. As shown in Fig. 5a, the baseline SEC (without any improvement in selectivity) is estimated to be 6.38 GJ/t_{CO2}. When only CO_2/N_2 selectivity is increased

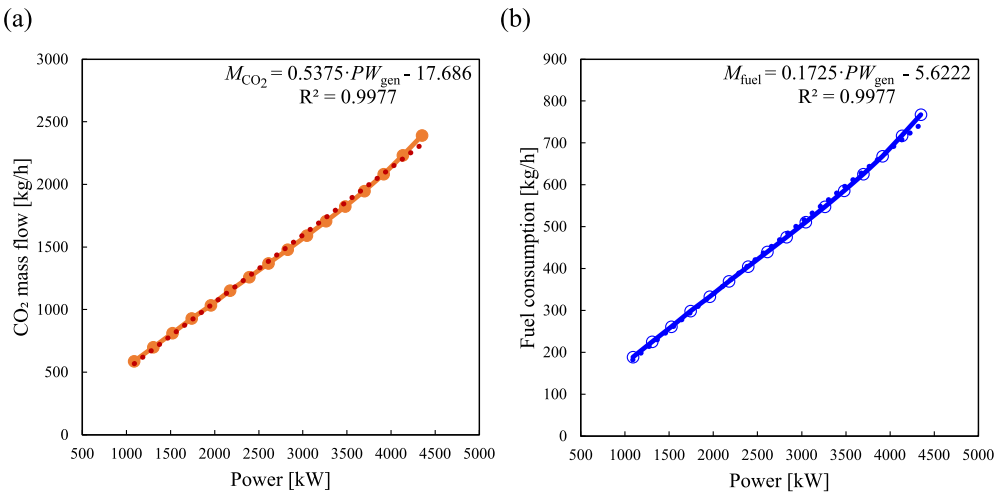

Fig. 4. Generator data as a function of power: (a) CO_2 mass flow; (b) Fuel consumption.

Table 8
Cost estimation for the process.

Category	Estimation formula	Unit	Ref
Membrane cost	$I_m = A_{mem} \bullet 50$	$	[18,22]
Membrane frame cost	$I_{mf} = (A_{mem}/2000)^{0.7} \bullet 2.38 \bullet 10^5$	$	[18,22]
Vacuum pump cost	$I_{vp} = \dot{m}_{inlet} \bullet 1.578 \bullet 10^4$	$	[18,45]
Compressor cost: 3–9 bar	$I_{cp} = \dot{m}_{inlet} \bullet 0.387 \bullet 10^4$	$	[18,45]
Compressor cost: 9–27 bar	$I_{cp} = \dot{m}_{inlet} \bullet 0.048 \bullet 10^5$	$	[18,45]
Compressor cost: 27–81 bar	$I_{cp} = \dot{m}_{inlet} \bullet 0.096 \bullet 10^5$	$	[18]
Cooler cost	$I_{clr} = 3.5 \bullet 10^6 \bullet V_{std}/440$	$	[18]
Multi heat exchanger cost	$I_{he} = 12003 \bullet A^{0.603} \bullet 1.011187^{Pr} \bullet 1.08$	$	[43]
Separator cost	$I_{sep} = 70693 \bullet V^{0.562} \bullet 1.015215^{Pr} \bullet 1.08$	$	[43]
Dryer cost	$I_{dry} = 90 \bullet M_{water} \bullet 1.08$	$	[43]
Equipment cost	$I_{equip} = I_{vp} + I_{cp} + I_{clr} + I_{he} + I_{sep} + I_{dry}$	–	–
Depreciation factor (25 years)	$d = 0.064$	–	[18,45]
Depreciation factor (5 years)	$d_m = 0.225$	–	[18,45]
Annualized capital cost	$C_{ACAPEX} = (I_{equip} + I_{mf}) \bullet d + I_m \bullet d_m$	$/year	[18,45]
Annual O&M cost	$C_{O\&M} = 0.036 \bullet I_{equip} + 0.01 \bullet (I_m + I_{mf})$	$/year	[18,45]
Annual fuel cost	C_{fuel} = Annul fuel consumption • Fuel cost	$/year	[46]
Annual OPEX	$C_{OPEX} = C_{O\&M} + C_{fuel}$	$/year	–
Total annual cost	$C_{total} = C_{ACAPEX} + C_{OPEX}$	$/year	–
CO_2 avoidance cost	$C_{avoided} = C_{total}$/Annual CO_2 avoided	$/$t_{avoided}$	[14]

by 100 %, the SEC decreases to 4.74 GJ/t_{CO2} (point A), representing a 25.7 % reduction. Similarly, increasing CO_2/O_2 selectivity from 4 to 8 results in a SEC of 4.96 GJ/t_{CO2} (point B, with a reduction of 22.3 %). However, when both selectivities are improved by 100 %, the SEC is considerably reduced to 3.27 GJ/t_{CO2}. At this point (point C), the CO_2/N_2 selectivity reaches approximately 24, and the CO_2/O_2 selectivity reaches 8, leading to an overall 50 % reduction in SEC. Furthermore, the SEC contour lines exhibit a convex shape toward the origin at point O, suggesting that balanced CO_2/N_2 and CO_2/O_2 selectivity results in lower SEC values compared with cases where one selectivity is disproportionately high.

Table 9
Optimization variables.

Category	Unit	Lower bound	Upper bound	Remark
CO_2 permeance	GPU	1000	3000	Capture
MEM 1 stage cut	fraction	0	1	Capture
MEM 2 stage cut	fraction	0	1	Capture
MEM 3 stage cut	fraction	0	1	Capture
Pressure ratio at Comp 1	–	0	4	Liquefaction
Pressure ratio at Comp 2	–	0	4	Liquefaction
Pressure ratio at Comp 3	–	0	4	Liquefaction
Pr1	bar	16	30	Liquefaction

Table 10
Optimization constraints.

Category	Remark
CO_2 temperature ≥ -55.0 ℃	T1, T2
WtW GHG intensity ≤ 62.90 g_{CO2eq}/MJ	

Fig. 5b illustrates the CO_2 avoidance costs required to achieve 62.90 g_{CO2eq}/MJ. The baseline cost of CO_2 avoidance, with no improvement in selectivity, is \$308.9/t_{CO2}. A 100 % improvement in CO_2/N_2 selectivity alone reduces the cost by 28.8 % to \$219.9/t_{CO2}, whereas a 100 % improvement in CO_2/O_2 selectivity results in a 24.8 % reduction to \$232.4/t_{CO2}. When both selectivities are improved by 100 %, the avoidance cost decreases remarkably to \$155.3/t_{CO2} (49.7 % reduction). Recent proposals suggest that a GHG emission fee of between \$150 and \$300 per tonne of CO_2 could be introduced [47,48]. For CCS to be a financially viable alternative to carbon tax, the CO_2 avoidance cost should ideally remain below \$150 per ton of CO_2. As depicted in Fig. 5b, this target is nearly met at point C. Currently, MTR's Polaris membrane has a CO_2/N_2 selectivity of 50, twice the required selectivity of 24 [20]. However, CO_2/O_2 selectivity is not explicitly stated. Since most polymeric membranes exhibit a CO_2/O_2 selectivity of at least 4, achieving a selectivity of 8 appears to be feasible through material engineering, particularly by optimizing gas-selective free volume distributions. Therefore, the necessary selectivity levels seem attainable with existing membrane technology, making membrane-based CCS systems a promising solution for meeting the 2040–2044 regulatory limits.

The major reasons for cost reduction can be explained in two ways: operating expenditure (OPEX) and capital expenditure (CAPEX). In the

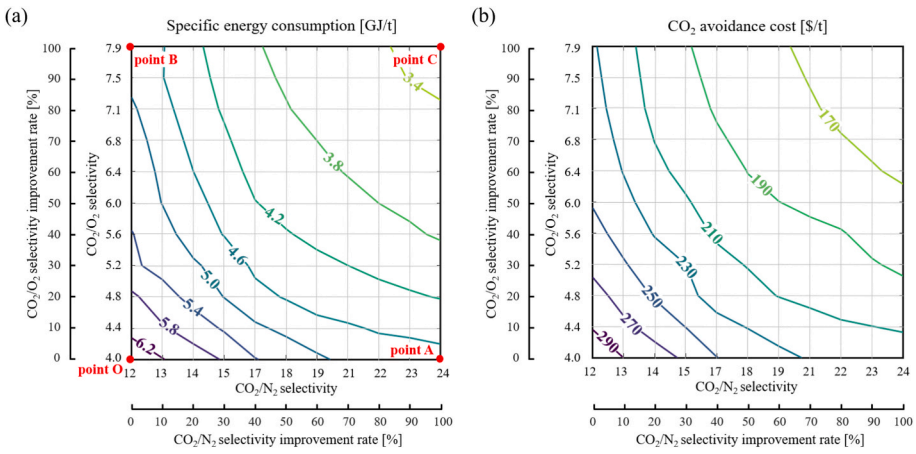

Fig. 5. Effects of improvement in CO_2/N_2 and CO_2/O_2 selectivity, satisfying the GHG intensity limit of 62.90 g_{CO2eq}/MJ: (a) Specific energy consumption; (b) CO_2 avoidance cost.

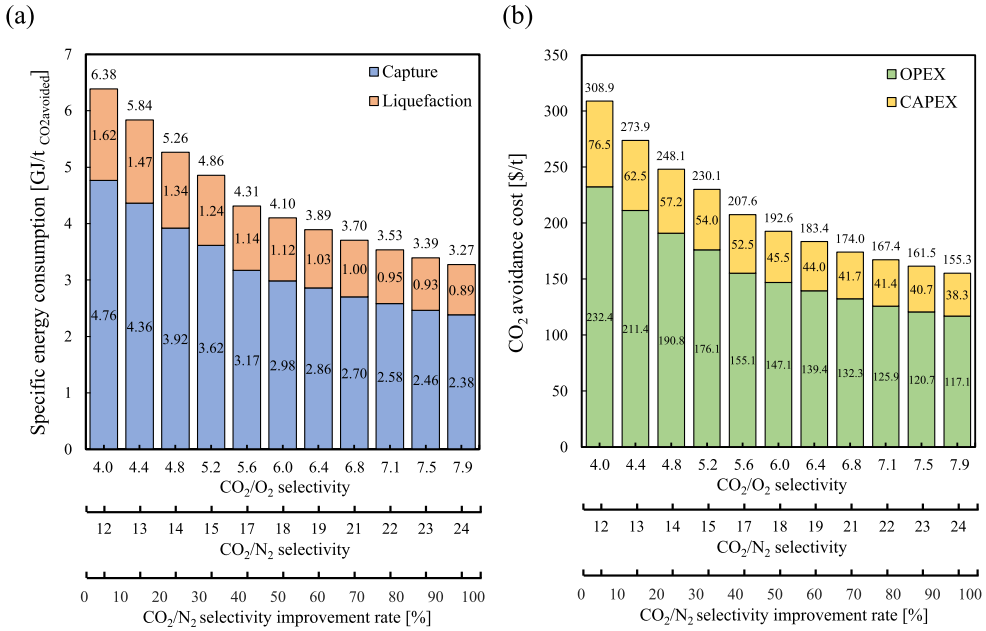

Fig. 6. Effects of both improvement in CO_2/N_2 and CO_2/O_2 selectivity, satisfying the GHG intensity limit of 62.90 g_{CO2eq}/MJ: (a) Specific energy consumption for capture and liquefaction; (b) CAPEX and OPEX of the OCCS system.

base case without selectivity enhancements, the energy consumption for capture and liquefaction was 4.76 and 1.62 GJ/t_{CO2}, respectively (Fig. 6a). With 100 % selectivity improvements, these values dropped to 2.38 and 0.89 GJ/t_{CO2}, approximately 50 % reduction in both cases. This reduction in energy consumption directly contributes to a decrease in the OPEX (Fig. 6b). As selectivity improves, the reduction in energy consumption leads to lower fuel consumption, subsequently reducing the OPEX. Since a reduction in the capture energy is expected, it is necessary to analyze the decrease in the liquefaction energy. The presence of impurities, such as oxygen and nitrogen, lowers the dew point of the mixture, requiring lower temperatures for liquefaction and increasing the overall energy demand. However, as membrane separation performance improves, the liquefaction inlet CO_2 purity (y_{CO_2}) rises, reducing the amount of gas recycled back to the membrane capture process from the first separator during liquefaction (M_{rec}). This leads to a lower liquefaction inlet mass flow ($M_{liq,in}$) (Fig. 7). As a result, the overall energy required for liquefaction decreases.

Fig. 8 provides a detailed breakdown of the CAPEX and OPEX for an individual membrane unit and CO_2 liquefaction system as a function of membrane performance. The enhanced membrane performance reduces the CAPEX (Fig. 6b). As shown in Fig. 8a, the membrane unit consistently accounts for over 79 % of the total CAPEX, regardless of membrane performance. At baseline membrane performance, the CAPEX was approximately \$65.54/t_{CO2} but decreased to approximately \$30.14/t_{CO2} with a 100 % improvement in membrane performance, representing a cost reduction of over 50 %. This reduction stems primarily from the decreased membrane area requirement due to the increased CO_2 permeance (Table B. 3). In contrast, the CAPEX for the liquefaction system experienced a smaller reduction of approximately 26 %, declining from \$10.96/t_{CO2} to \$8.12/t_{CO2} with a 100 % improvement in membrane performance. This limited decrease is due to the minimal change in the volumetric flow of the captured gas entering the liquefaction system, despite the increase in CO_2 purity (Fig. 7).

It is worth noting that, as the membrane performance improves, the impact on the CO_2 avoidance cost and SEC reduction gradually diminishes (Fig. 6 and Fig. 8). Initially, enhancements in CO_2 /N_2 and CO_2/O_2 selectivities led to considerable reductions in cost and SEC. However, with further improvements, the rate of reduction slowed

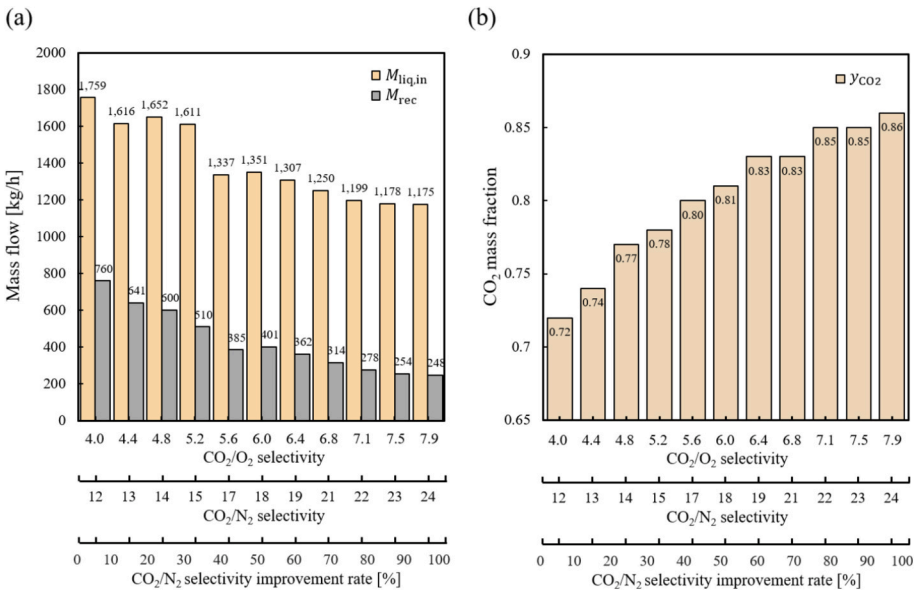

Fig. 7. Effects of both improvement in CO_2/N_2 and CO_2/O_2 selectivity, satisfying the GHG intensity limit of 62.90 g_{CO2eq}/MJ: (a) Liquefaction inlet mass flow ($\boldsymbol{M}_{liq.in}$) and recycle mass flow ($\boldsymbol{M}_{rec}$); (b) Liquefaction inlet CO_2 purity ($\boldsymbol{y}_{CO_2}$).

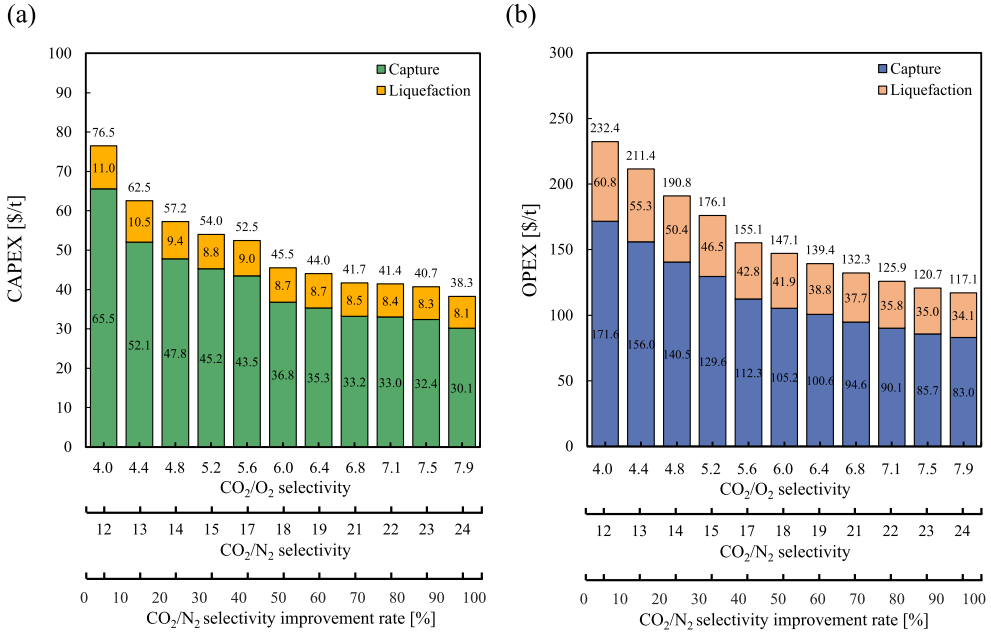

Fig. 8. Effects of both improvement in CO_2/N_2 and CO_2/O_2 selectivity, satisfying the GHG intensity limit of 62.90 g_{CO2eq}/MJ: (a) CAPEX for capture and liquefaction process; (b) OPEX for capture and liquefaction process.

Table 11
Target GHG intensity limit.

Reduction rate (%)	GHG intensity limit (g_{CO2eq}/MJ)	Remark
Reference	91.16	FuelEU maritime reference
14.5	77.94	2035–2039 target in FuelEU maritime
31	62.90	2040–2044 target in FuelEU maritime
40	54.70	
50	45.58	

down. A similar trend was observed when only CO_2/O_2 selectivity was enhanced while keeping CO_2/N_2 selectivity constant, and vice versa (Fig. 5). These findings suggest inherent limitations to further reducing costs and SEC solely through improvements in membrane selectivity.

4.2. Case study with different target greenhouse gas intensity

To estimate the effect of target GHG intensity, four target GHG intensity levels were selected corresponding to reduction rates of 14.5 % (2035–2039 target), 31 % (2040–2044 target), 40 %, and 50 % from the reference value of 91.16 g_{CO2eq}/MJ based on FuelEU Maritime regulations (Table 11).With the WtW GHG intensity constraint, optimization was performed to minimize the CO_2 avoidance cost.

Fig. 9. Presents the results of a case studysatisfying the target GHG

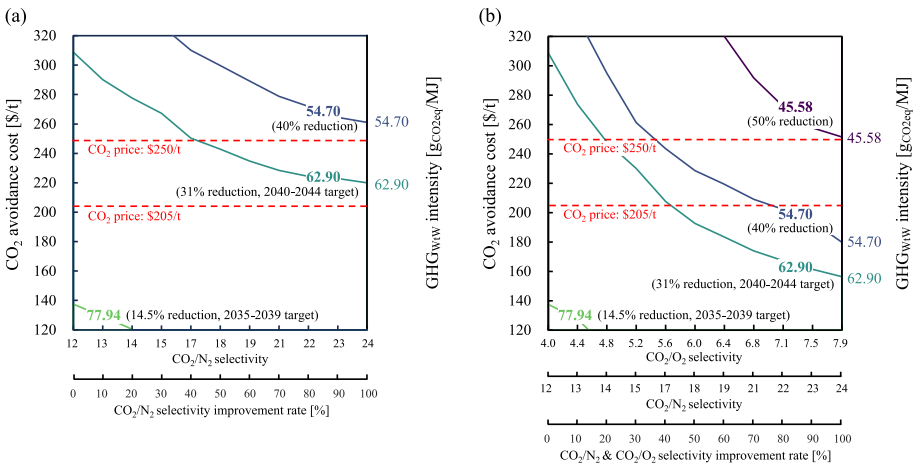

Fig. 9. Effects of improving selectivity on GHG intensity and CO_2 avoidance cost: (a) improving CO_2/N_2 selectivity; (b) improving both CO_2/N_2 and CO_2/O_2 selectivity.

intensity. Fig. 9a shows the results when only CO_2/N_2 selectivity is improved, whereas Fig. 9b illustrates the effects of improving both CO_2/N_2 and CO_2/O_2 selectivities. These results provide information on the level of CO_2/N_2 and CO_2/O_2 selectivity that is appropriate for meeting target GHG intensity with a reasonable CO_2 avoidance cost.

In line with advanced economics with net-zero emissions pledges by 2050, CO_2 prices will be \$205/t_{CO2} in 2040 and \$250/t_{CO2} in 2050 [49]. Under these carbon price scenarios, the level of selectivity improvement required to achieve the target GHG intensity varies. The results show that the current membrane without improvement can satisfy the GHG intensity target of 77.94 g_{CO2eq}/MJ with a CO_2 avoidance cost of \$137.52/t_{CO2}, which is lower than the assumed CO_2 price of \$205/t_{CO2}, as shown in Fig. 9. However, to satisfy the GHG limit of 62.90 g_{CO2eq}/MJ, the avoidance cost of \$205/t_{CO2} cannot be achieved by improving CO_2/N_2 selectivity only (Fig. 9). To achieve an avoidance cost of \$250/t_{CO2}, a minimum improvement of 40 % in CO_2/N_2 selectivity is required to comply with the 62.90 g_{CO2eq}/MJ target. These results indicate that improving CO_2/N_2 selectivity alone may be insufficient to meet the more stringent GHG intensity limits.

When the CO_2/N_2 and CO_2/O_2 selectivities are simultaneously improved, the requirements for economic feasibility and compliance with the GHG intensity limits were less stringent. Achieving the avoidance cost of \$205/t_{CO2} with a GHG intensity target of 62.90 g_{CO2eq}/MJ requires a 50 % improvement in both selectivities. A stricter GHG target of 54.70 g_{CO2eq}/MJ can be satisfied with an 80 % improvement in CO_2/N_2 and CO_2/O_2 selectivities. Achieving an avoidance cost of \$250/t_{CO2} requires less stringent selectivity improvement. To meet the target values of 62.90 and 54.70 g_{CO2eq}/MJ, improvements of 20 and 40 % in CO_2/N_2 and CO_2/O_2 selectivities, respectively, are sufficient. Though, achieving the 45.58 g_{CO2eq}/MJ limit requires CO_2/N_2 and CO_2/O_2 selectivities exceeding 24 and 8, respectively, which are still attainable for polymeric membranes. This suggests that membrane-based carbon capture systems can be competitive in marine applications if designed to account for higher O_2 concentrations.

4.3. Sensitivity analysis

A parametric sensitivity analysis was conducted across a representative range of selectivity (0.5–1.0) to assess its impact on SEC and CO_2 avoidance cost (Fig. 10) [50]. The potential variation in CO_2/H_2O selectivity due to membrane hydrophobicity or hydrophilicity was not considered.

As the selectivity increases, the SEC decreases from 3.57 GJ/t_{CO2} to 3.25 GJ/t_{CO2}. The selectivity has the most significant impact on the membrane area and the power consumption of the vacuum pump in the

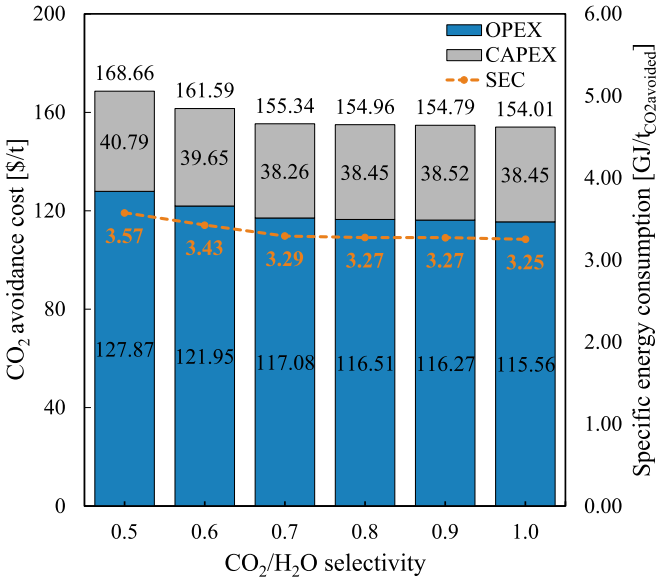

Fig. 10. Variations of CO_2 avoidance cost and specific energy consumption with CO_2/H_2O selectivity.

first membrane stage. At lower selectivity, more water permeates through the membrane, requiring a larger membrane area and higher vacuum pump energy consumption. However, the rate of improvement diminishes beyond a selectivity of 0.7. This is because most of the water is removed by the downstream separator installed after the first membrane stage. Regardless of the CO_2/H_2O selectivity, the mole fraction of H_2O in the gas stream after the separator is consistently reduced to approximately 0.05, indicating that further improvements in selectivity yield limited additional benefit in terms of energy consumption. Similarly, the total CO_2 avoidance cost decreases from \$168.66/t_{CO2} at a selectivity of 0.5 to \$154.01/t_{CO2} at a selectivity of 1.0. This reduction is mainly due to lower OPEX; decreased energy consumption reduces fuel usage, while the CAPEX remains relatively constant across the range. These results indicate that enhancing membrane selectivity toward CO_2 over H_2O can improve process efficiency and reduce operational costs; however, the marginal benefit becomes less significant at higher selectivity values due to downstream water removal.

Fuel consumption has the most significant impact on operating OPEX; consequently, fluctuations in fuel prices substantially affect the capture cost. Fuel prices are influenced by a variety of external factors,

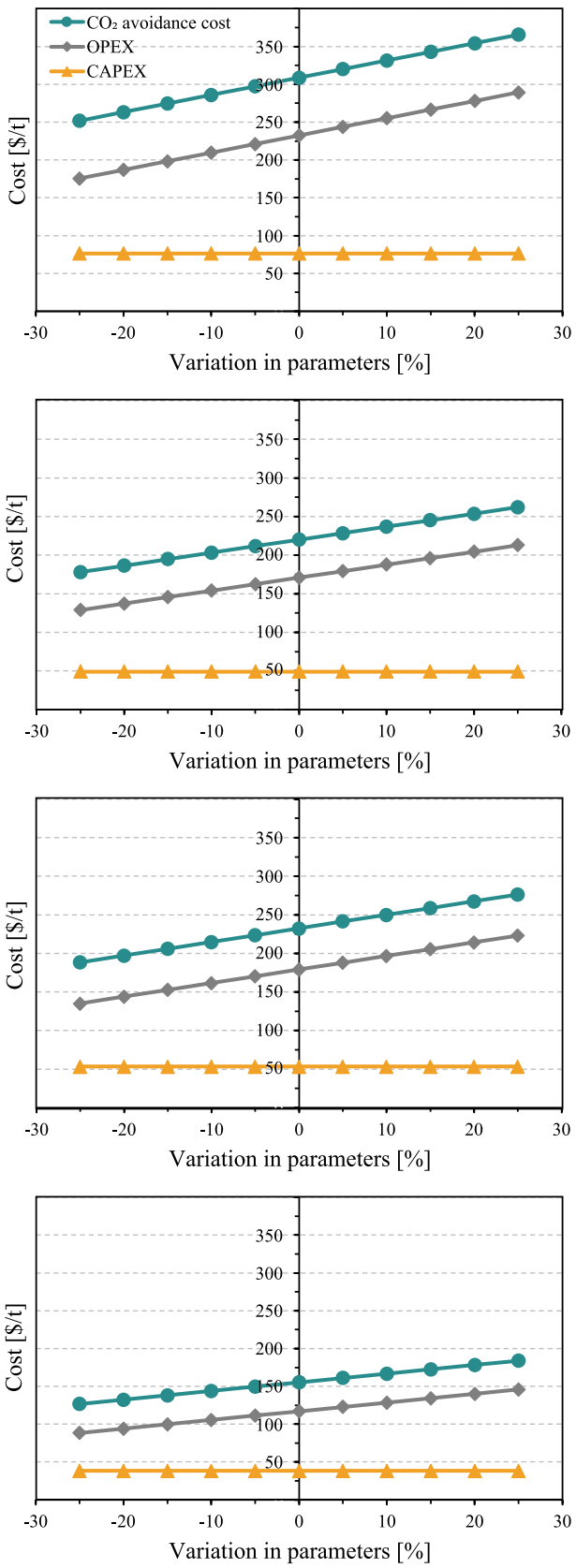

Fig. 11. Variations of CO_2 avoidance cost, OPEX and CAPEX with fuel price: (a) base case (without selectivity improvement); (b) 100% improvement in CO_2/N_2 selectivity; (c) 100% improvement in CO_2/O_2 selectivity; (d) 100% improvement in both CO_2/N_2 and CO_2/O_2 selectivity.

including geopolitical conditions, exchange rates, global oil prices, and global wars.

To assess the impact of fuel price variation on the capture cost, a sensitivity analysis was conducted. The analysis was based on the fuel price assumption of \$774/t as presented in Section 3.5, and the price varied from − 25 % to + 25 %. Four cases were considered: the base case (without selectivity improvement), 100 % improvement in CO_2/N_2 selectivity, 100 % improvement in CO_2/O_2 selectivity, and 100 % improvement in both CO_2/N_2 and CO_2/O_2 selectivity. All other parameters remained constant, and the analysis was conducted under the target GHG intensity of 62.90 gCO_{2eq}/MJ, as shown in Fig. 11.

In all cases, the CO_2 avoidance cost varied by approximately − 18 % to + 18 % in response to fuel price fluctuations. For the base case, the avoidance cost ranged from \$251.9/t_{CO2} to \$365.8/t_{CO2}. If the MGO price is relatively low, a reasonable avoidance cost can be achieved even in the base case. However, at higher fuel prices, the base case becomes economically unattractive. Conversely, in the final case of a 100 % improvement in both selectivities, the avoidance cost remains relatively low, even at the highest fuel price of \$967.5/t, yielding a cost of \$184.0/t_{CO2}. This is still below the CO_2 price of \$205/t and \$250/t assumed in Section 4.2, indicating economic feasibility.

Since fuel consumption is a dominant factor in the overall CO_2 avoidance cost, optimizing energy consumption is crucial. Enhancing the membrane process to reduce energy demand or developing high-performance membrane materials, such as CO_2/O_2-selective membranes, can make the system more energy-efficient. Such improvements can ensure the feasibility of onboard carbon capture and storage systems even under volatile fuel price conditions.

Increasing the pressure ratio enhances the driving force across the membrane, which leads to improved CO_2 recovery. However, this also causes stress on the membrane material, potentially reducing its durability. Given the importance of membrane durability, a sensitivity analysis was conducted to evaluate the impact of membrane lifespan on the CO_2 avoidance cost, while keeping all other parameters constant.

Using an interest rate of 4 % and applying the annual capital charge ratio as referenced in the cost estimation section 3.5, the sensitivity analysis varied the membrane lifespan from 2.5 to 7.5 years (±50 % of the assumption). The resulting variation in CO_2 avoidance cost ranged from −2.5 % to + 7.4 % across all cases, as shown in Fig. 12. Specifically, the avoidance cost changed from \$332.2/t to \$301.1/t, \$230.9/t to \$216.3/t, \$245.2/t to \$228.1/t, and \$164.2/t to \$152.4/t for the four scenarios. These results indicate that a shortened membrane replacement interval can increase the CO_2 avoidance cost by up to 7.4 %, highlighting the significance of carefully selecting the operating pressure.

5. Conclusions

This study shows that improving CO_2/N_2 and CO_2/O_2 selectivities is inevitable for membrane-based CO_2 capture on ships. A three-stage membrane system integrating a precooled Linde–Hampson liquefaction process was optimized to minimize CO_2 avoidance costs while complying with FuelEU Maritime regulations. Two case studies were conducted to assess the impact of improving CO_2/N_2 and CO_2/O_2 selectivities. The first case targeted a fixed GHG intensity of 62.90 g_{CO2eq}/MJ to meet the 2040–2044 goal, while the second targeted varying GHG intensities. In the first case, a 100 % improvement in CO_2/N_2 selectivity alone reduces the SEC by 25.7 % (from 6.38 to 4.74 GJ/t_{CO2}) and the CO_2 avoidance cost by 28.8 % (from \$308.9 to \$219.9/t_{CO2}). However, improving both the CO_2/N_2 and CO_2/O_2 selectivities results in a more significant reduction—in SEC by 48.7 % (down to 3.27 GJ/t_{CO2}) and in cost by 49.7 % (down to \$155.3/t_{CO2}), highlighting the crucial role of CO_2/O_2 selectivity. In the second case, under a CO_2 price of \$250/t_{CO2}, the baseline selectivity (without improvement) meets the 77.94 g_{CO2eq}/MJ GHG target, but achieving stricter targets requires substantial selectivity improvements. Reaching 62.90 g_{CO2eq}/MJ necessitates at

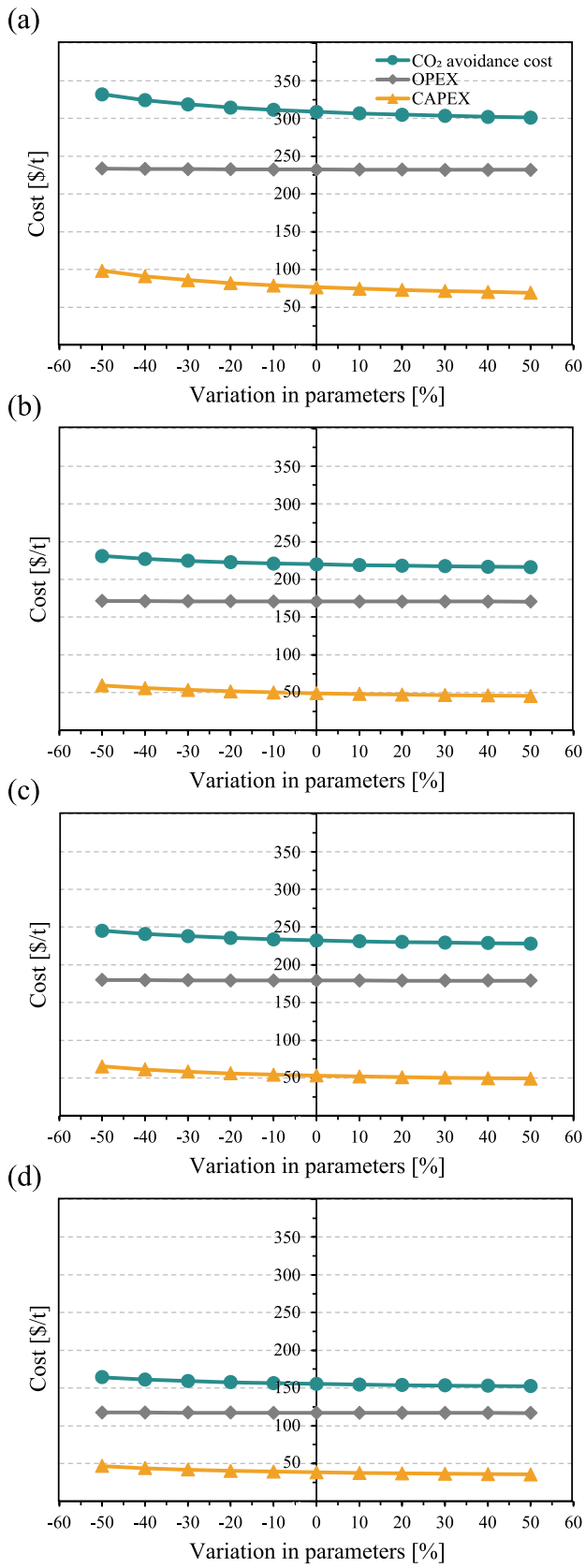

Fig. 12. Variations of CO_2 avoidance cost, OPEX and CAPEX with membrane life span: (a) base case (without selectivity improvement); (b) 100% improvement in CO_2/N_2 selectivity; (c) 100% improvement in CO_2/O_2 selectivity; (d) 100% improvement in both CO_2/N_2 and CO_2/O_2 selectivity.

least a 40 % increase in CO_2/N_2 selectivity or a 20 % improvement in both CO_2/N_2 and CO_2/O_2 selectivities, while the 54.70 g_{CO2eq}/MJ target demands a 40 % enhancement in both. To reach the most stringent target of 45.58 g_{CO2eq}/MJ, improvements of over 100 % in both the CO_2/N_2 and CO_2/O_2 selectivities are required. These findings confirm that CO_2/N_2 selectivity alone is insufficient to meet stringent GHG limits and CO_2/O_2 selectivity must also be enhanced concurrently. Moreover, achieving 100 % improvements in CO_2/N_2 and CO_2/O_2 selectivities of 24 and 8, respectively, is realistically attainable through polymeric membrane material engineering. These suggest that membrane-based CO_2 capture can be a viable and competitive solution for maritime applications.

Declaration of generative AI and AI-assisted technologies in the writing process

The authors wrote the draft of paper, and used ChatGPT in order to only improve the readability. After using this tool, the authors reviewed and edited the content as needed and take(s) full responsibility for the content of the published article.

CRediT authorship contribution statement

Hongkyoung Shin: Writing – original draft, Visualization, Methodology, Investigation, Formal analysis, Conceptualization. **Abduljelil Worku Sabir:** Visualization, Methodology, Investigation. **Juyoung Oh:** Validation, Methodology. **Pyung soo Lee:** Writing – review & editing, Supervision, Formal analysis, Conceptualization. **Youngsub Lim:** Writing – review & editing, Supervision, Resources, Methodology, Funding acquisition, Formal analysis, Conceptualization.

Declaration of competing interest

The authors declare the following financial interests/personal relationships which may be considered as potential competing interests: Youngsub Lim reports financial support was provided by Korea Institute of Marine Science and Technology Promotion. If there are other authors, they declare that they have no known competing financial interests or personal relationships that could have appeared to influence the work reported in this paper.

Acknowledgments

This research was supported by Korea Institute of Marine Science & Technology Promotion (KIMST) funded by the Ministry of Oceans and Fisheries (2520000449), Korea Institute for Advancement of Technology (KIAT) grant funded by the Korea Government (MOTIE) (P0023684 HRD Program for Industrial Innovation), and the Korea Research Institute of Ships and Ocean engineering, grant from Endowment Project of "Technology Development of Onboard Carbon Capture and Storage System and Pilot Test" funded by Ministry of Oceans and Fisheries (PES5480).

Appendix A. . Process selection of the onboard carbon capture and storage system

Both two-stage (Fig A. 1) and three-stage (Fig. 3) membrane capture processes were designed for the selected engine, and optimization was performed to minimize CO_2 avoidance cost while satisfying the greenhouse gas intensity limit of 62.90 gCO_{2eq}/MJ.

The CO_2 purity of the stream entering the liquefaction process is 58 mol% for the two-stage case and 63 mol% for the three-stage case, and the liquefied CO_2 purity is 97 mol% in both cases. The presence of impurities such as oxygen and nitrogen lower the dew point, increasing

energy demand for liquefaction. Recycle mass flow from liquefaction to the membrane process is higher in the two-stage case (986.54 kg/h) compared to the three-stage case (759.99 kg/h), which increases overall process mass flow and results in higher energy consumption in both capture and liquefaction units. The larger membrane area required for the two-stage process is primarily due to this increased recycle flow (Table A. 1).

As a result, the three-stage membrane process was selected because it achieves the required CO_2 purity and greenhouse gas intensity limit with a simpler configuration and lower capital and operating costs under the given engine conditions.

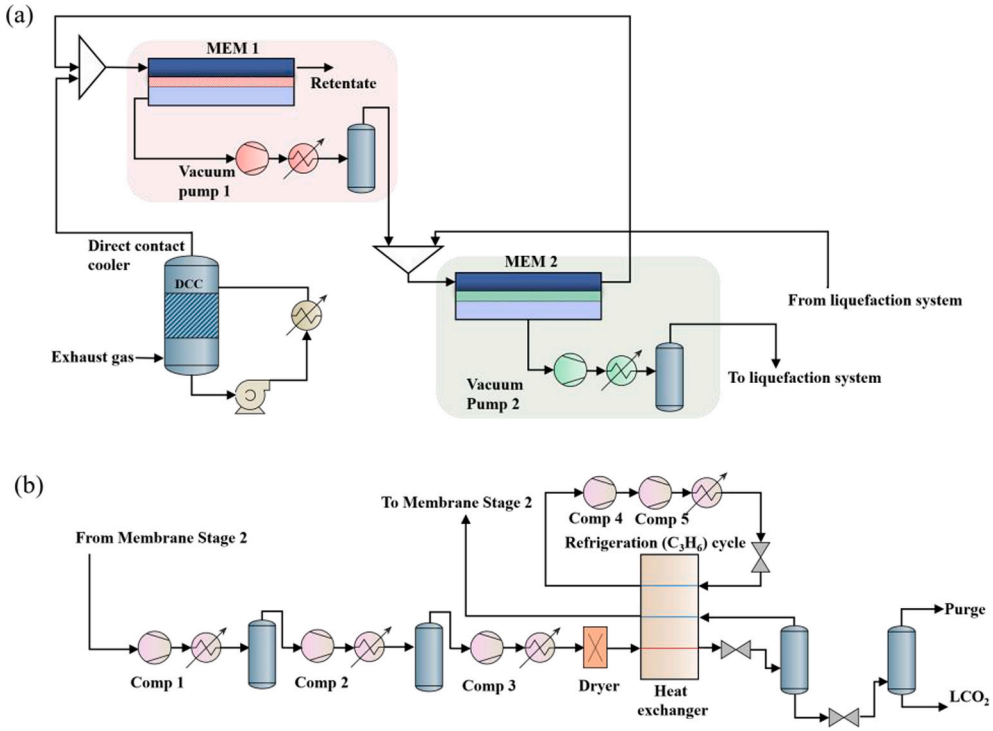

Fig. A1. Process flow diagram of the 2-stage onboard membrane carbon capture and storage system.

Table A1
Performance comparison of the 2-stage and 3-stage onboard membrane capture and storage system.

Category	Unit	2-stage	3-stage
1st membrane area	m^2	6090.07	4259.52
2nd membrane area	m^2	1078.00	716.19
3rd membrane area	m^2	–	898.88
Total membrane cost	$	471,441	386,369
Total electric energy	kW	897.38	855.68
Capture energy	kW	655.01	638.52
Liquefaction energy	kW	242.37	217.16
Fuel consumption for required electricity	t/y	1110.77	1057.20
Annual Fuel cost	$/y	859,735	818,274
CO_2 avoidance cost	$/$t_{CO2}$	346.98	308.86
CAPEX	$/$t_{CO2}$	89.54	76.49
OPEX	$/$t_{CO2}$	257.44	232.37

Appendix B. . Membrane separation performance

.

Table B1
Membrane separation performance at different improvement rates for CO_2/N_2 selectivity.

Improvement rate (%)	CO_2/N_2 selectivity	CO_2 permeance (GPU)
0	12.0	1600
10	12.5	2400
20	13.5	2642
30	14.5	2800
40	15.6	2836

(*continued on next page*)

Table B1 (*continued*)

Improvement rate (%)	CO_2/N_2 selectivity	CO_2 permeance (GPU)
50	16.7	2891
60	17.9	2800
70	19.1	2642
80	20.3	2642
90	21.1	3000
100	22.2	3000

Table B2
Membrane separation performance at different improvement rates for CO_2/O_2 selectivity.

Improvement rate (%)	CO_2/O_2 selectivity	CO_2 permeance (GPU)
0	4.0	1600
10	4.3	2110
20	4.7	2110
30	5.1	1674
40	5.5	2100
50	5.9	2115
60	6.3	2600
70	6.7	1800
80	7.1	2400
90	7.5	1950
100	7.9	2475

Table B3
Membrane separation performance at different improvement rates for CO_2/N_2 and CO_2/O_2 selectivities.

Improvement rate (%)	Selectivity		CO_2 permeance (GPU)
	CO_2/N_2	CO_2/O_2	
0	12.0	4.0	1600
10	12.6	4.3	2300
20	13.7	4.7	2300
30	14.9	5.1	2300
40	16.3	5.5	2023
50	16.9	5.9	2636
60	18.0	6.3	2700
70	18.9	6.7	2871
80	20.2	7.1	2716
90	21.4	7.5	2657
100	22.2	7.8	3000

Appendix C. . Supplementary data for CO_2/O_2-selective membrane

Table C1
Experimental data for CO_2/O_2-selective membrane.

Category	$P(CO_2)$ barrers	$\alpha(CO_2/N_2)$	$\alpha(CO_2/O_2)$	Ref
Poly[bis(2-(2-methoxyethoxy)ethoxy)phosphazene]	250	62.5	35.7	[51]
Modified poly (dimethylsiloxane)	2000	34.2	11.4	[52]
PIM-PI-9	2180	23.2	7.4	[53]
PIM-PI-1	1100	23.4	7.3	[54]
PIM-1	2300	25	6.2	[55]
PIM-7	1100	26	5.8	[55]

.

Data availability

No data was used for the research described in the article.

References

[1] DNV, Energy Transition Outlook 2024: Maritime Forecast to 2050, 2024.
[2] IMO, Report of the Marine Environment Protection Committee on its Eighty-First Session, 2024.
[3] IMO, Resolution MEPC.376 (80); Guidelines on life cycle GHG intensity of marine fuels (LCA Guidelines), 2023.

[4] Korean Register, KR GEARs Key Updates, (2023). http://kr-decarbonization.co.kr/2023/winter/eng/inside.html (accessed September 23, 2024).
[5] Korean Register, IMO Regulatory Trends, (2024). http://kr-decarbonization.co.kr/2024/summer/eng/regulatory.html (accessed September 23, 2024).
[6] European Commission, Regulation of the European Parliament and of the Council on the use of renewable and low-carbon fuels in maritime transport, and amending. Directive 2009/16/EC, 2023.
[7] DNV, Energy Transition Outlook 2023: Maritime Forecast to 2050, 2023.
[8] A. Awoyomi, K. Patchigolla, E.J. Anthony, Process and economic evaluation of an onboard capture system for LNG-fueled CO_2 carriers, Ind. Eng. Chem. Res. 59 (2020) 6951–6960, https://doi.org/10.1021/acs.iecr.9b04659.
[9] S. Lee, S. Yoo, H. Park, J. Ahn, D. Chang, Novel methodology for EEDI calculation considering onboard carbon capture and storage system, Int. J. Greenhouse Gas Control 105 (2021), https://doi.org/10.1016/j.ijggc.2020.103241.
[10] J.A. Ros, E. Skylogianni, V. Doedée, J.T. van den Akker, A.W. Vredeveldt, M.J. G. Linders, E.L.V. Goetheer, J.-G.-M.-S. Monteiro, Advancements in ship-based carbon capture technology on board of LNG-fuelled ships, Int. J. Greenhouse Gas Control 114 (2022), https://doi.org/10.1016/j.ijggc.2021.103575.
[11] ABS, LNG as Marine Fuel, 2022.
[12] ABS, Carbon Neutral Fuel Pathways and Transformational Technologies, 2024.
[13] Korean Register, The Evolution of Alternative Ship Fuels and Fuel Containment Systems, (2023). http://kr-decarbonization.co.kr/2023/autumn/eng/insights.html#insights2 (accessed 23 September 2024).
[14] J. Oh, D. Kim, S. Roussanaly, R. Anantharaman, Y. Lim, Optimal capacity design of amine-based onboard CO_2 capture systems under variable marine engine loads, Chem. Eng. J. 483 (2024), https://doi.org/10.1016/j.cej.2024.149136.
[15] X. Luo, M. Wang, Study of solvent-based carbon capture for cargo ships through process modelling and simulation, Appl. Energy 195 (2017) 402–413, https://doi.org/10.1016/j.apenergy.2017.03.027.
[16] M. Cho, Y. Seo, E. Park, D. Chang, S. Han, Process design and energy assessment of an onboard carbon capture system with boilers or heat pumps for additional steam generation, Ships Offshore Struct. 19 (2024) 1309–1322, https://doi.org/10.1080/17445302.2023.2243687.
[17] R. Notz, H.P. Mangalapally, H. Hasse, Post combustion CO_2 capture by reactive absorption: pilot plant description and results of systematic studies with MEA, Int. J. Greenhouse Gas Control 6 (2012) 84–112, https://doi.org/10.1016/j.ijggc.2011.11.004.
[18] J.P. Van Der Sluijs, C.A. Hendriks, K. Blok, Feasibility of polymer membranes for carbon dioxide recovery from flue gases, Energy Convers. Manag. 33 (1992) 429–436, https://doi.org/10.1016/0196-8904(92)90040-4.
[19] D.F. Sanders, Z.P. Smith, R. Guo, L.M. Robeson, J.E. McGrath, D.R. Paul, B. D. Freeman, Energy-efficient polymeric gas separation membranes for a sustainable future: a review, Polymer 54 (2013) 4729–4761, https://doi.org/10.1016/j.polymer.2013.05.075.
[20] T.C. Merkel, H. Lin, X. Wei, R. Baker, Power plant post-combustion carbon dioxide capture: an opportunity for membranes, J. Memb. Sci. 359 (2010) 126–139, https://doi.org/10.1016/j.memsci.2009.10.041.
[21] S. Lee, M. Binns, J.K. Kim, Automated process design and optimization of membrane-based CO_2 capture for a coal-based power plant, J. Memb. Sci. 563 (2018) 820–834, https://doi.org/10.1016/j.memsci.2018.06.057.
[22] J. Xu, Z. Wang, Z. Qiao, H. Wu, S. Dong, S. Zhao, J. Wang, Post-combustion CO_2 capture with membrane process: Practical membrane performance and appropriate pressure, J. Memb. Sci. 581 (2019) 195–213, https://doi.org/10.1016/j.memsci.2019.03.052.
[23] M. Feenstra, J. Monteiro, J.T. van den Akker, M.R.M. Abu-Zahra, E. Gilling, E. Goetheer, Ship-based carbon capture onboard of diesel or LNG-fuelled ships, Int. J. Greenhouse Gas Control 85 (2019) 1–10, https://doi.org/10.1016/j.ijggc.2019.03.008.
[24] J. Oh, R. Anantharaman, U. Zahid, P.S. Lee, Y. Lim, Process design of onboard membrane carbon capture and liquefaction systems for LNG-fueled ships, Sep. Purif. Technol. 282 (2022), https://doi.org/10.1016/j.seppur.2021.120052.
[25] L.M. Robeson, B.D. Freeman, D.R. Paul, B.W. Rowe, An empirical correlation of gas permeability and permselectivity in polymers and its theoretical basis, J. Memb. Sci. 341 (2009) 178–185, https://doi.org/10.1016/j.memsci.2009.06.005.
[26] P. Rallapalli, K.P. Prasanth, D. Patil, R.S. Somani, R.V. Jasra, H.C. Bajaj, Sorption studies of CO_2, CH_4, N_2, CO, O_2 and ar on nanoporous aluminum terephthalate [MIL-53(Al)], J. Porous Mater. 18 (2011) 205–210, https://doi.org/10.1007/s10934-010-9371-7.
[27] A.W. Thornton, B.D. Freeman, L.M. Robeson, Polymer Gas Separation Membrane Database, (2012). https://research.csiro.au/virtualscreening/membrane-database-polymer-gas-separation-membranes/ (accessed 11 October 2024).
[28] L.M. Robeson, The upper bound revisited, J. Memb. Sci. 320 (2008) 390–400, https://doi.org/10.1016/j.memsci.2008.04.030.
[29] J.A. Chavez Velasco, R. Tumbalam Gooty, M. Tawarmalani, R. Agrawal, Optimal design of membrane cascades for gaseous and liquid mixtures via MINLP, J. Memb. Sci. 636 (2021), https://doi.org/10.1016/j.memsci.2021.119514.
[30] S.E. Demirel, J. Li, M.M.F. Hasan, Membrane Separation process design and intensification, Ind. Eng. Chem. Res. 60 (2021) 7197–7217, https://doi.org/10.1021/acs.iecr.0c05072.
[31] Y. Seo, C. Huh, S. Lee, D. Chang, Comparison of CO2 liquefaction pressures for ship-based carbon capture and storage (CCS) chain, Int. J. Greenhouse Gas Control 52 (2016) 1–12, https://doi.org/10.1016/j.ijggc.2016.06.011.
[32] Y. Seo, H. You, S. Lee, C. Huh, D. Chang, Evaluation of CO_2 liquefaction processes for ship-based carbon capture and storage (CCS) in terms of life cycle cost (LCC) considering availability, Int. J. Greenhouse Gas Control 35 (2015) 1–12, https://doi.org/10.1016/j.ijggc.2015.01.006.
[33] J. Oh, D. Kim, S. Roussanaly, Y. Lim, Greenhouse gas emissions of shipping with onboard carbon capture under the FuelEU Maritime regulation: a well-to-wake evaluation of different propulsion scenarios, Chem. Eng. J. 498 (2024), https://doi.org/10.1016/j.cej.2024.155407.
[34] WINGD, General Technical Data 2.23.0.0, 2024.
[35] R.W. Baker, T. Merkel, B.C. Freeman, Large pilot testing of the MTR, Membrane Post-Combustion CO2 Capture Process (2018).
[36] E. Favre, Carbon dioxide recovery from post-combustion processes: can gas permeation membranes compete with absorption? J. Memb. Sci. 294 (2007) 50–59, https://doi.org/10.1016/j.memsci.2007.02.007.
[37] R. Bounaceur, N. Lape, D. Roizard, C. Vallieres, E. Favre, Membrane processes for post-combustion carbon dioxide capture: a parametric study, Energy 31 (2006) 2556–2570, https://doi.org/10.1016/j.energy.2005.10.038.
[38] D. Keairns, R. Newby, V. Shah, M. Turner, M. Woods, Current and Future Technologies for Power Generation with Post-combustion Carbon Capture – Final Report (2012). Doi: 10.2172/1489757.
[39] H. Takaba, S. Nakao, Computational fluid dynamics study on concentration polarization in H2/CO separation membranes, J. Memb. Sci. 249 (2005) 83–88, https://doi.org/10.1016/j.memsci.2004.09.038.
[40] US Department of Energy National Energy Technology Laboratory, Large Pilot Testing of the MTR Membrane Post-Combustion CO_2 Capture Process primary project goals, 2018.
[41] Y. Huang, T.C. Merkel, R.W. Baker, Pressure ratio and its impact on membrane gas separation processes, J. Memb. Sci. 463 (2014) 33–40, https://doi.org/10.1016/j.memsci.2014.03.016.
[42] M. Cakartas, J. Zhou, J. Ren, A. Andreasen, H. Yu, Techno-economical evaluation and comparison of various CO_2 transportation pathways, Comput. Aided Chem. Eng. 53 (2024) 2077–2082, https://doi.org/10.1016/B978-0-443-28824-1.50347-1.
[43] H. Deng, S. Roussanaly, G. Skaugen, Techno-economic analyses of CO_2 liquefaction: impact of product pressure and impurities, Int. J. Refrig 103 (2019) 301–315, https://doi.org/10.1016/j.ijrefrig.2019.04.011.
[44] R.K. Pachauri, A. Reisinger, Synthesis Report. Contribution of Working Groups I, II and III to the Fourth Assessment Report of the Intergovernmental Panel on Climate Change, Geneva, Switzerland, 2007.
[45] D. Yang, Z. Wang, J. Wang, S. Wang, Potential of two-stage membrane system with recycle stream for CO_2 capture from post combustion gas, Energy Fuels 23 (2009) 4755–4762, https://doi.org/10.1021/ef801109p.
[46] Bunker Index, Bunker Index: Rotterdam, Netherlands, (2024). https://bunkerindex.com/index.php (accessed 16 July 2024).
[47] Korean Register, Methanol as Marine Fuel, 2023.
[48] ABS, Setting the Course to Low Carbon Shipping, 2022.
[49] International Energy Agency, Global Energy and Climate Model Documentation 2024, 2024.
[50] Q. Li, H. Wu, Z. Wang, J. Wang, Analysis and optimal design of membrane processes for flue gas CO_2 capture, Sep. Purif. Technol. 298 (2022), https://doi.org/10.1016/j.seppur.2022.121584.
[51] C. Orme, M. Harrup, T. Luther, R. Lash, K. Houston, D. Weinkauf, F. Stewart, Characterization of gas transport in selected rubbery amorphous polyphosphazene membranes, J. Memb. Sci. 186 (2001) 249–256, https://doi.org/10.1016/S0376-7388(00)00690-6.
[52] U. Senthilkumar, B. Reddy, Polysiloxanes with pendent bulky groups having amino-hydroxy functionality: structure-permeability correlation, J. Memb. Sci. 292 (2007) 72–79, https://doi.org/10.1016/j.memsci.2007.01.014.
[53] Y. Rogan, L. Starannikova, V. Ryzhikh, Y. Yampolskii, P. Bernardo, F. Bazzarelli, J. C. Jansen, N.B. McKeown, Synthesis and gas permeation properties of novel spirobisindane-based polyimides of intrinsic microporosity, Polym. Chem. 4 (13) (2013) 3813–3820, https://doi.org/10.1039/c3py00451a.
[54] B.S. Ghanem, N.B. McKeown, P.M. Budd, J.D. Selbie, D. Fritsch, High-performance membranes from polyimides with intrinsic microporosity, Adv. Mater. 20 (14) (2008) 2766–2771, https://doi.org/10.1002/adma.200702400.
[55] P.M. Budd, K.J. Msayib, C.E. Tattershall, B.S. Ghanem, K.J. Reynolds, N. B. McKeown, D. Fritsch, Gas separation membranes from polymers of intrinsic microporosity, J. Memb. Sci. 251 (2005) 263–269, https://doi.org/10.1016/j.memsci.2005.01.009.